


Article

# MnBi<sub>2</sub>Se<sub>4</sub>-Based Magnetic Modulated Heterostructures

Evgeniy K. Petrov <sup>1,2,\*</sup> , Vladimir M. Kuznetsov <sup>1</sup> and Sergey V. Ereemeev <sup>1,3</sup> 

<sup>1</sup> Laboratory of Nanostructured Surfaces and Coatings, Tomsk State University, 634050 Tomsk, Russia; kuznetsov@rec.tsu.ru (V.M.K.); eremeev@ispms.tsc.ru (S.V.E.)

<sup>2</sup> Laboratory of Electronic and Spin Structure of Nanosystems, St. Petersburg State University, 199034 St. Petersburg, Russia

<sup>3</sup> Institute of Strength Physics and Materials Science, Russian Academy of Sciences, 634055 Tomsk, Russia

\* Correspondence: evg.konst.petrov@gmail.com

**Abstract:** Thin films of magnetic topological insulators (TIs) are expected to exhibit a quantized anomalous Hall effect when the magnetizations on the top and bottom surfaces are parallel and a quantized topological magnetoelectric effect when the magnetizations have opposite orientations. Progress in the observation of these quantum effects was achieved earlier in the films with modulated magnetic doping. On the other hand, the molecular-beam-epitaxy technique allowing the growth of stoichiometric magnetic van der Waals blocks in combination with blocks of topological insulator was developed. This approach should allow the construction of modulated heterostructures with the desired architecture. In the present paper, based on the first-principles calculations, we study the electronic structure of symmetric thin film heterostructures composed of magnetic MnBi<sub>2</sub>Se<sub>4</sub> blocks (septuple layers, SLs) and blocks of Bi<sub>2</sub>Se<sub>3</sub> TI (quintuple layers, QLs) in dependence on the depth of the magnetic SLs relative to the film surface and the TI spacer between them. Among considered heterostructures we have revealed those characterized by nontrivial band topology.

**Keywords:** topological insulators; magnetism; density functional theory calculations



**Citation:** Petrov E.K.; Kuznetsov, V.M.; Ereemeev, S.V. MnBi<sub>2</sub>Se<sub>4</sub>-Based Magnetic Modulated Heterostructures. *Magnetism* **2022**, *2*, 1–9. <https://doi.org/10.3390/magnetism2010001>

Academic Editor: Xichao Zhang

Received: 2 December 2021

Accepted: 27 December 2021

Published: 4 January 2022

**Publisher's Note:** MDPI stays neutral with regard to jurisdictional claims in published maps and institutional affiliations.



**Copyright:** © 2022 by the authors. Licensee MDPI, Basel, Switzerland. This article is an open access article distributed under the terms and conditions of the Creative Commons Attribution (CC BY) license (<https://creativecommons.org/licenses/by/4.0/>).

## 1. Introduction

The combination of nontrivial band topology and magnetism gives rise to novel spintronic phenomena, such as the quantum anomalous Hall effect and the topological magnetoelectric effect. The defining features of the quantum anomalous Hall (QAH) effect [1] is the appearance of the quantized Hall resistivity ( $\rho_{yx}$ ) and vanishing longitudinal resistivity ( $\rho_{xx}$ ) in the absence of an external magnetic field. A necessary condition for this is the band gap opening in the Dirac surface state of a topological insulator (TI) due to the exchange interaction between the surface electrons and the magnetic moments perpendicular to the surface. The QAH effect was observed first for the molecular beam epitaxy (MBE) grown (Bi,Sb)<sub>2</sub>Te<sub>3</sub> TI thin films doped with magnetic elements such as chromium [2–7] and vanadium [8,9]. However, the observed temperature of the QAH effect in such films was limited to below 300 mK due to the inhomogeneity of the coupling between the surface Dirac electrons and the dopants' magnetic moments. Later, it was reported that the QAH effect was observed at 1 K, which was achieved by the construction of modulated thin TI films where magnetic doping (Cr) was organized only in certain quintuple layers (QLs) of (Bi<sub>1–y</sub>Sb<sub>y</sub>)<sub>2</sub>Te<sub>3</sub> [10]. Such modulated doping enhanced the magnetically induced gap in the TI surface Dirac state due to a higher Cr doping concentration as well as the reduction of the doping induced disorder on the TI surface. The topological magnetoelectric (TME) effect is another quantization phenomenon [11,12] due to which the magnetization of a material can be induced by an external electric field, and electric polarization can be induced by an external magnetic field. In order to observe the TME effect, the magnetizations are required to point inwards or outwards from the surface so that all the TI surfaces are gapped and the 3D TI becomes an insulator, termed an axion insulator (AXI). The TME effect can also occur in thin films with the anti-parallel magnetization alignment at the top and

bottom surfaces [13,14]. The axion insulator state was realized in the modulation-doped magnetic heterostructures prepared by the layer-by-layer MBE with Cr in the vicinity of the top and bottom surfaces of the  $(\text{Bi}_{1-y}\text{Sb}_y)_2\text{Te}_3$  with the asymmetric location of the magnetic layer [15] and in asymmetric films where a nonmagnetic layer of  $(\text{Bi}_{1-y}\text{Sb}_y)_2\text{Te}_3$  is sandwiched by a Cr-doped and V-doped layers [16].

However, there is an alternative way to combine magnetism with TI which provides even more magnetic homogeneity than magnetic modulated doping, that is, the formation of van der Waals heterostructures based on magnetic and topological insulators. Van der Waals materials offer a platform that allows the creation of heterostructures (including those composed of topological and magnetic materials) with a variety of properties [17–21]. The magnetic topological van der Waals heterostructure was experimentally realized for the first time by self-organized incorporation of an MnSe bilayer inside  $\text{Bi}_2\text{Se}_3$ , resulting in the formation of an  $\text{MnBi}_2\text{Se}_4/\text{Bi}_2\text{Se}_3$  heterostructure [22]. Similar heterostructures composed of a magnetic septuple layer (SL)  $\text{MnBi}_2\text{Te}_4$  or  $\text{CrBi}_2\text{Se}_4$  on top of TIs have been proposed theoretically, called TI magnetic extension heterostructures [23–25]. Furthermore,  $\text{MnBi}_2\text{Te}_4$  bulk crystals were found to be an intrinsic antiferromagnetic topological insulator (AFM TI) [26–31]. It allows us to observe a number of exotic states of matter and phenomena such as quantized magnetoelectric coupling [31], axion insulator state [27,28,32], and various Hall effects [27,28,31–36]. A family of V-containing planar AFM TI compounds was also theoretically proposed [37]. A homologous series of  $(\text{MnBi}_2\text{Te}_4)\cdot(\text{Bi}_2\text{Te}_3)_n$  stoichiometric bulk materials [38–45], in which the  $\text{MnBi}_2\text{Te}_4$  SLs are periodically separated by  $n$  QLs of  $\text{Bi}_2\text{Te}_3$ , demonstrate tunable interlayer exchange coupling depending on  $n$ . Similar  $(\text{MnSb}_2\text{Te}_4)\cdot(\text{Sb}_2\text{Te}_3)_n$  magnetic materials with non-trivial band topology were recently proposed theoretically [46]. Relatively thick films composed of  $\text{MnBi}_2\text{Se}_4$  and  $\text{Bi}_2\text{Se}_3$ , or  $\text{MnBi}_2\text{Te}_4$  and  $\text{Bi}_2\text{Te}_3$  with random distribution of the magnetic SLs as well as a novel magnetic heterostructure  $\text{Mn}_4\text{Bi}_2\text{Te}_7/\text{Bi}_2\text{Te}_3$  were experimentally fabricated by MBE [47–49]. However, precise layer-by-layer MBE growth based on the self-organized incorporation of an Mn monolayer [22] potentially allows the preparation of ordered van der Waals heterostructures, composed of SL blocks of  $\text{MnBi}_2\text{Se}_4$ ,  $\text{MnBi}_2\text{Te}_4$  and  $\text{MnSb}_2\text{Te}_4$  antiferromagnetic compounds [50] separated by QLs of related  $\text{Bi}_2\text{Se}_3$ ,  $\text{Bi}_2\text{Te}_3$ , and  $\text{Sb}_2\text{Te}_3$  TIs, structurally similar to those in the modulated magnetic-doped films.

In the present study, using the state-of-the-art DFT calculations, we theoretically scrutinize an interplay between magnetism and topology in symmetric thin films composed of magnetic  $\text{MnBi}_2\text{Se}_4$  SL blocks and QLs of  $\text{Bi}_2\text{Se}_3$  TI in dependence on the depth of magnetic SLs and the width of the TI spacer between them. We found that thin film heterostructures, in which the magnetic SL blocks are placed on top of or near the surface with at least a 3QL thick TI spacer, are potential candidates for realizing topological edge states within a relatively large band gap. On the other hand, the heterostructures in which the TI spacer is thin or absent and magnetic SL blocks are buried deep under the surface are characterized by a small (or even absent) hybridization gap and are topologically trivial.

## 2. Materials and Methods

The calculations were carried out using the projector augmented-wave method (PAW) [51] implemented in the VASP package [52–54]. The exchange-correlation effects were taken into account using Perdew–Burke–Ernzerhof generalized gradient approximation (GGA) [55]. Spin-orbit coupling was treated using the second variation method [56]. The DFT-D3 method [57] was used to accurately describe the van der Waals interaction. All slab calculations were carried out within the repeating slabs model with a vacuum layer thickness of 10 Å. All considered crystal structure parameters were optimized until ionic forces became less than  $10^{-2}$  eV/Å. It should be noted that, in bulk material, the thickness of  $\text{Bi}_2\text{Se}_3$  QL blocks is  $\approx 9.549$  Å, and the thickness of  $\text{MnBi}_2\text{Se}_4$  SL blocks is  $\approx 12.602$  Å. However, the thickness of the top QL (SL) blocks in the relaxed heterostructures becomes different compared to their thickness in the bulk  $\text{Bi}_2\text{Se}_3$  ( $\text{MnBi}_2\text{Se}_4$ ). The difference magnitude is not large, although it is significant. Plane wave energy cutoff was set to  $E_{cut} = 280$  eV and was kept constant through all calculations. Edge band structures were calculated within

the tight-binding approach based on maximally localized Wannier functions [58–60] using the iterative Green’s function method [61] implemented in the WannierTools package [62]. Mn 3*d*-states were treated using the GGA+*U* approach [63,64]. The adopted value of  $U_{\text{eff}} = 5.24$  eV was set to the one determined for bulk MnSe [65]. This value was also compared to the one calculated using the linear response method [66] and they were found to be similar. Chern numbers were calculated using Z2pack [67,68].

### 3. Results

In the present study, we consider heterostructures consisting of MnBi<sub>2</sub>Se<sub>4</sub> and Bi<sub>2</sub>Se<sub>3</sub> blocks stacked along the [0001] direction with MnBi<sub>2</sub>Se<sub>4</sub> SLs located at different depths from the surface. First, we would like to establish a nomenclature we could use to refer to certain heterostructure configurations. For brevity, we will denote the magnetic block as M and the number of TI blocks numerically. Thus, in general form, *mMnMm* means a symmetric film containing two magnetic MnBi<sub>2</sub>Se<sub>4</sub> SL blocks covered with *m* QL blocks of Bi<sub>2</sub>Se<sub>3</sub> TI with an *n* QLs spacer placed between magnetic SLs. At that, *m* and *n* can take on a zero value. As an example, we show the structure of 1M3M1 film, that is, QL-SL-QL-QL-QL-SL-QL, in Figure 1a.

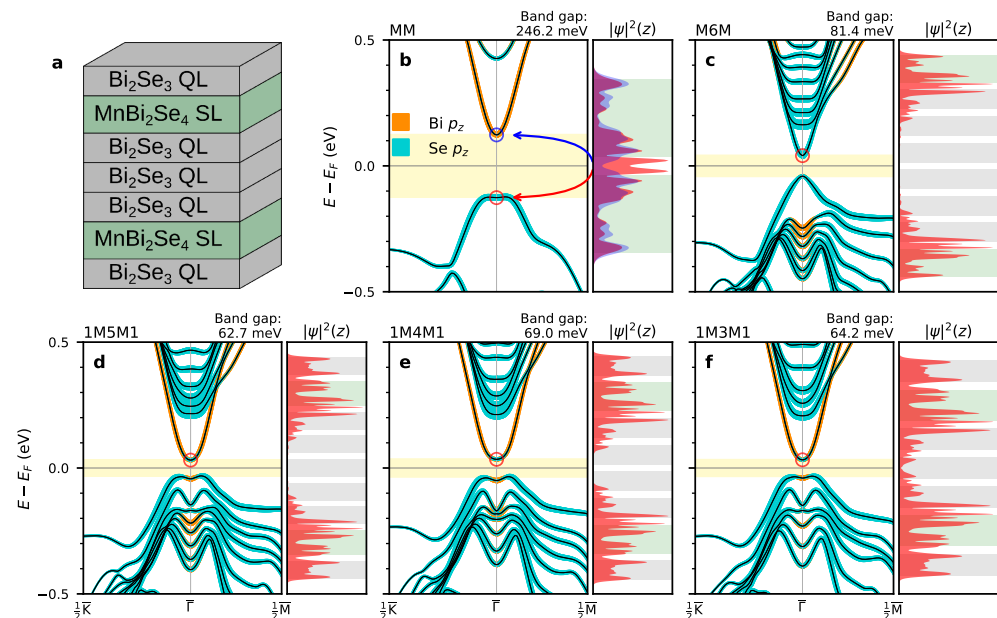


**Figure 1.** (a) Schematic structure of the MnBi<sub>2</sub>Se<sub>4</sub>-based modulated *mMnMm* heterostructures (1M3M1 case is shown as an example). (b–f, left side) Calculated band structures of the MM, M6M, 1M5M1, 1M4M1, and 1M3M1 heterostructures near the Fermi level. The black lines represent the dispersion curves. The color lines (see the legend in panel b) correspond to the weight of Bi and Se  $p_z$  orbitals. Yellow stripes in the spectra mark the band gap. (b–f, right side) Spatial localization of the states marked in the spectra with circles of the same colors.

First, we consider the simplest MM case ( $m = n = 0$ ), which corresponds to an isolated 2 SL slab of antiferromagnetic MnBi<sub>2</sub>Se<sub>4</sub>. As can be seen from Figure 1b (left panel), in this case the band structure exhibits  $\approx 250$  meV band gap. The orbital composition of the band gap edges, which demonstrate that the top of the valence band is formed by Se  $p_z$  orbitals and the bottom of the conduction band occupied by Bi  $p_z$  orbitals, suggests that there is no band gap inversion. This is confirmed by the Chern number  $C$  calculation, which shows  $C = 0$ . In the artificial FM configuration (which can be achieved in the external magnetic field), the band structure remains topologically trivial ( $C = 0$ ). A similar situation has been observed in a 2 SL slab of MnSb<sub>2</sub>Te<sub>4</sub> [46]. In contrast, a 2 SL slab of MnBi<sub>2</sub>Te<sub>4</sub>, being topologically trivial in the AFM state, in the FM configuration exhibits non-trivial band topology and possesses axion insulator phase [27]. At the opposite extreme, when magnetic MnBi<sub>2</sub>Se<sub>4</sub> SL blocks are separated by a sufficiently thick TI spacer of six QLs (Figure 1c

(left panel)), we have the M6M heterostructure which has been studied earlier [22]. This symmetric heterostructure is characterized by the non-zero Chern number which shows that this is a QAH phase. It should be noted that the band gap in the Dirac state of  $\approx 81$  meV remains the same in the asymmetric “M6” heterostructure. This indicates that the magnetic SL blocks do not interact with each other in the M6M heterostructure. Both the large band gap in the Dirac state and the absence of interaction of the states of opposite surfaces stem from their spacial localization (Figure 1c, right panel). The gapped Dirac state is located mainly in the outer SLs that provides its effective hybridization with Mn orbitals, and states localized on the top and bottom surfaces of the film do not overlap with each other. It is obvious that a small decrease in the TI spacer thickness (e.g., by one QL block) will not affect the spectrum and band topology.

Next we consider  $1MnM1$  heterostructures in which the magnetic  $MnBi_2Se_4$  SLs are buried under  $Bi_2Se_3$  QL (similar to Cr-doped modulated films [10]) with variation of TI spacer width  $n$  from 5 to 3 QLs. In these cases, the band structures have a lot in common and exhibit indirect band gaps ranging from 62 to 69 meV (Figure 1d–f, left panels). Another common feature of the  $1MnM1$  heterostructures is the spatial localization of the gapped Dirac state (Figure 1d–f, right panels). It is almost equally distributed in the outer QL and subsurface SL blocks. Compared to the M6M heterostructure, the weight of the state in the magnetic block is decreased, which results in a smaller magnetic gap. It should be noted that decreasing  $n$  from 5 to 3 QLs does not result in an overlap of the Dirac states localized on the opposite surfaces of the film. The orbital composition of the band gap edges suggests the band gap inversion, that is, in the  $\Gamma$  point vicinity the valence band top is mainly formed by Bi  $p_z$  orbitals, while away from the  $\Gamma$  it is mainly Se  $p_z$  orbitals. On the other hand, the conduction band is rather equally formed by both Bi and Se  $p_z$  orbitals. The  $1MnM1$  heterostructures, when Mn magnetic moments on the top and bottom sides of the film are oppositely oriented, are found to be topologically trivial according to the Chern number calculation. When Mn magnetic moments in both SLs are oriented parallel, all considered  $1MnM1$  films exhibit no significant change in the band spectra (the band gaps are 65.8, 67.9 and 66.4 meV for  $n = 5, 4, 3$ , respectively), but show non-trivial band topology with Chern number  $C = 1$ . Hence, in these cases it is possible to observe the quantum Hall effect in the external magnetic field without Landau levels. On the other hand,  $1MnM1$  heterostructures, being topologically trivial insulators in an antiparallel magnetic configuration and showing  $C = 1$  under external magnetic field, change the sign of the Chern number to  $-1$  when FM magnetization is reversed, indicating an AXI topological phase. Earlier, the QAH state was observed in the modulated heterostructure of a similar architecture with Cr doping introduced in the second (subsurface) QL of topological insulator film where an undoped TI spacer between Cr-doped blocks of four QLs [10]. It was found that the QAH state in the given film with immersed magnetic block is more stable than that in the heterostructure with a magnetic block on top. In contrast, our results show no advantage for structures with immersed magnetic block and hence it is rather due to technical limitations in the MBE-grown heterostructures. Our results also demonstrate weak dependence of the electronic structure of  $1MnM1$  films on  $n$  ranging from 3 to 5 QLs.

Figure 2 shows the edge band spectra of the  $1M3M1$  film cut along the (110) crystallographic plane with different magnetization directions on opposite surfaces, antiparallel, when the film possesses the topologically trivial phase, and parallel, when it exhibits non-trivial band topology. The edge electronic structure of the topologically trivial phase (Figure 2a) demonstrates the gapped spectrum while being switched into the topological phase, characterized by the  $C = 1$ , the film possesses a single linear spin-polarized state crossing the Fermi level (Figure 2b).

Now we consider  $2M3M2$ ,  $2M2M2$  and  $2M1M2$  heterostructures in which  $MnBi_2Se_4$  SLs are buried under two  $Bi_2Se_3$  QLs and separated by 3, 2 and 1  $Bi_2Se_3$  QLs, respectively. In these heterostructures the electronic spectra are rather different. They exhibit narrow band gaps of 17 meV, 20.6 meV and 17.9 meV for  $2M3M2$ ,  $2M2M2$  and  $2M1M2$  cases, respectively (see Figure 3a–c, left panels), for antiparallel orientation of Mn magnetic moments in top and bottom SLs. When the magnetization has the same direction in the top and bottom SLs

these gaps are similarly small or even absent. In both parallel and antiparallel Mn magnetic moments orientations, the band structures exhibit trivial band topology. The small gap at the Fermi level in these spectra emerges from hybridization of the Dirac state, localized primarily within the two outer QLs of  $\text{Bi}_2\text{Se}_3$ , like in pristine  $\text{Bi}_2\text{Se}_3$ -type topological insulators [69], and the hole-like parabolic band, which has maximum of localization in the SL blocks, see Figure 3a–c (right panels). The Dirac state is gapless in the 2M3M2 case. However, it acquires a band gap as the spacer thickness decreases (and overall film thickness) due to overlap of the topological states localized on opposite surfaces.

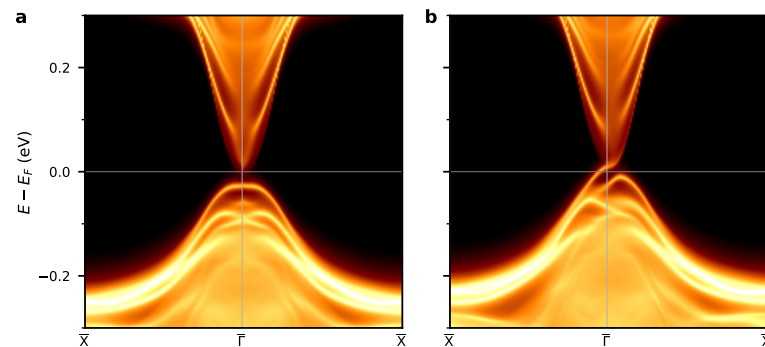


**Figure 2.** Calculated edge band structure in the 1M3M1 heterostructure with antiparallel (a) and parallel (b) magnetization in the  $\text{MnBi}_2\text{Se}_4$  SL blocks.

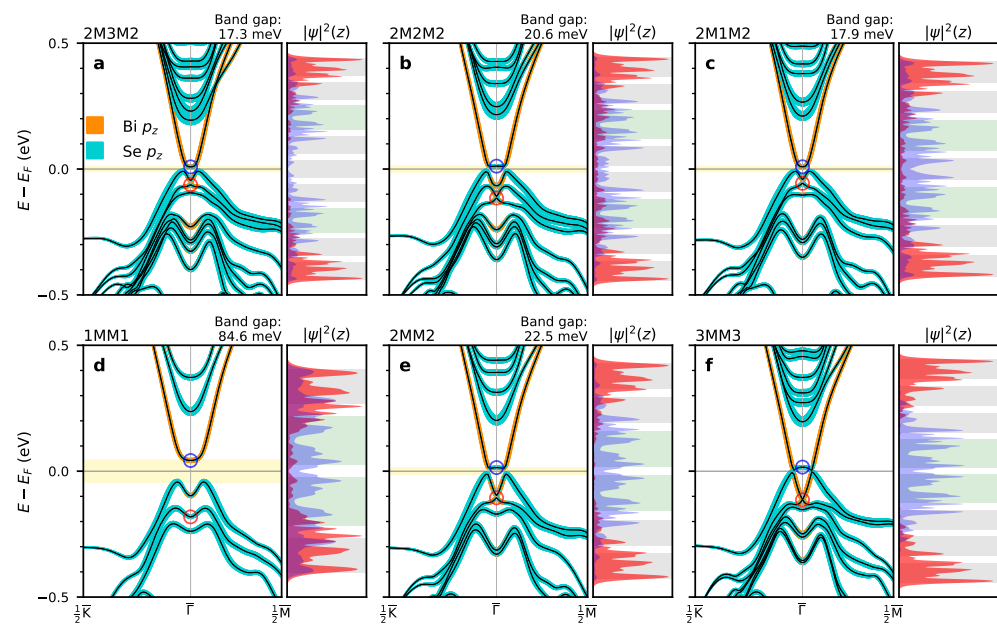


**Figure 3.** (a–f, left side) Calculated band structures of 2M3M2, 2M2M2, 2M1M2, 1MM1, 2MM2 and 3MM3 heterostructures and spatial localization of the states near the Fermi level. (b–f, right side) Spatial localization of the states marked in the spectra with circles of the same colors. The notations are the same as in Figure 1b–f.

Finally, we consider 1MM1, 2MM2 and 3MM3 heterostructures in which two SLs are located in the center (with spacer thickness  $n = 0$ ) and have a  $\text{Bi}_2\text{Se}_3$  “coat” of different thicknesses ( $m$  equals to 1, 2, and 3). In the 1MM1 case, when the AFM magnetic alignment of Mn spins is preserved (Figure 3d), the band structure exhibits an indirect band gap of  $\approx 85$  meV, which is almost three times less than in the MM film. The band gap becomes much smaller (20 meV) in the artificial FM configuration. As in the  $2MnM2$  heterostructures, this gap emerges due to hybridization between the surface Dirac states and the state predominantly localized in the SLs. However, in thin 1MM1 heterostructure this hybridization is much stronger. In the 2MM2 case, the band structure manifests an outline

of the Dirac cone (Figure 3e) and the hybridization gap at the Fermi level is noticeably smaller and comparable with those in the 2MnM2 heterostructures. In the 3MM3 case, the Dirac cone is completely formed with a clearly visible Dirac point at the  $\bar{\Gamma}$  point (Figure 3f). However, since the Dirac state is localized at the surface, it is practically independent from the MnBi<sub>2</sub>Se<sub>4</sub>-derived state near the Fermi level. Hence, they do not hybridize with each other resulting in the gapless spectrum. In the magnetic configuration with parallel magnetization of the two SL blocks, the 2MM2 and 3MM3 heterostructures exhibit metallic spectra. All these heterostructures, in which the TI spacer is small or absent and magnetic SL blocks are buried deep under TI coat, are topologically trivial regardless of the magnetization direction.

#### 4. Summary and Conclusions

In summary, we have studied the MnBi<sub>2</sub>Se<sub>4</sub>-based magnetic heterostructures of *mMnMm* architecture containing two magnetic MnBi<sub>2</sub>Se<sub>4</sub> SL blocks (M) covered with *m* QL blocks of Bi<sub>2</sub>Se<sub>3</sub> with *n* QL spacer are placed between magnetic SLs. Such heterostructures can be fabricated by precise layer-by-layer MBE growth based on the prefabricated Bi<sub>2</sub>Se<sub>3</sub> layers and Mn-Se co-deposition. These heterostructures, being based on van der Waals blocks of the stoichiometric magnetic compound MnBi<sub>2</sub>Se<sub>4</sub>, should demonstrate greater magnetic homogeneity than magnetic heterostructures with modulated doping, which should not impair the manifestations of non-trivial band topology by magnetic disorder. Based on the DFT calculations, we have scrutinized the electronic structure and topological invariants of these heterostructures in dependence on structure parameters *m* and *n*, as well as on magnetization directions in two magnetic SLs, antiparallel or parallel. Among the considered heterostructures, we revealed potential candidates for realizing topological phases. These prospective heterostructures are those containing magnetic SL blocks on top of or near the surface with a TI spacer not less than *n* = 3 QLs.

**Author Contributions:** Conceptualization, S.V.E. and E.K.P.; Investigation, E.K.P. and S.V.E.; Writing—Original draft preparation, E.K.P., V.M.K. and S.V.E.; Writing—Review and editing, S.V.E., V.M.K. and E.K.P.; project administration, S.V.E.; funding acquisition, S.V.E. All authors have read and agreed to the published version of the manuscript.

**Funding:** This work was supported by Russian Science Foundation (grant No. 18-12-00169-p).

**Acknowledgments:** Calculations were performed at the Research Park of Saint Petersburg State University “Computing Center” (<http://www.cc.spbu.ru/> accessed on 2 December 2021).

**Conflicts of Interest:** The authors declare no conflict of interest.

#### References

1. Haldane, F.D.M. Model for a Quantum Hall Effect without Landau Levels: Condensed-Matter Realization of the “Parity Anomaly”. *Phys. Rev. Lett.* **1988**, *61*, 2015–2018. doi: 10.1103/PhysRevLett.61.2015. [[CrossRef](#)] [[PubMed](#)]
2. Chang, C.Z.; Zhang, J.; Feng, X.; Shen, J.; Zhang, Z.; Guo, M.; Li, K.; Ou, Y.; Wei, P.; Wang, L.L.; et al. Experimental Observation of the Quantum Anomalous Hall Effect in a Magnetic Topological Insulator. *Science* **2013**, *340*, 167–170. doi: 10.1126/science.1234414. [[CrossRef](#)]
3. Checkelsky, J.G.; Yoshimi, R.; Tsukazaki, A.; Takahashi, K.S.; Kozuka, Y.; Falson, J.; Kawasaki, M.; Tokura, Y. Trajectory of the anomalous Hall effect towards the quantized state in a ferromagnetic topological insulator. *Nat. Phys.* **2014**, *10*, 731–736. doi: 10.1038/nphys3053. [[CrossRef](#)]
4. Kou, X.; Guo, S.T.; Fan, Y.; Pan, L.; Lang, M.; Jiang, Y.; Shao, Q.; Nie, T.; Murata, K.; Tang, J.; et al. Scale-Invariant Quantum Anomalous Hall Effect in Magnetic Topological Insulators beyond the Two-Dimensional Limit. *Phys. Rev. Lett.* **2014**, *113*, 137201. doi: 10.1103/PhysRevLett.113.137201. [[CrossRef](#)]
5. Kou, X.; Pan, L.; Wang, J.; Fan, Y.; Choi, E.S.; Lee, W.L.; Nie, T.; Murata, K.; Shao, Q.; Zhang, S.C.; et al. Metal-to-insulator switching in quantum anomalous Hall states. *Nat. Commun.* **2015**, *6*, 8474. doi: 10.1038/ncomms9474. [[CrossRef](#)]
6. Kandala, A.; Richardella, A.; Kempinger, S.; Liu, C.X.; Samarth, N. Giant anisotropic magnetoresistance in a quantum anomalous Hall insulator. *Nat. Commun.* **2015**, *6*, 7434. doi: 10.1038/ncomms8434. [[CrossRef](#)]
7. Feng, Y.; Feng, X.; Ou, Y.; Wang, J.; Liu, C.; Zhang, L.; Zhao, D.; Jiang, G.; Zhang, S.C.; He, K.; et al. Observation of the Zero Hall Plateau in a Quantum Anomalous Hall Insulator. *Phys. Rev. Lett.* **2015**, *115*, 126801. doi: 10.1103/PhysRevLett.115.126801. [[CrossRef](#)] [[PubMed](#)]

8. Chang, C.Z.; Zhao, W.; Kim, D.Y.; Zhang, H.; Assaf, B.A.; Heiman, D.; Zhang, S.C.; Liu, C.; Chan, M.H.W.; Moodera, J.S. High-precision realization of robust quantum anomalous Hall state in a hard ferromagnetic topological insulator. *Nat. Mater.* **2015**, *14*, 473–477. doi: 10.1038/nmat4204. [[CrossRef](#)] [[PubMed](#)]
9. Grauer, S.; Schreyeck, S.; Winnerlein, M.; Brunner, K.; Gould, C.; Molenkamp, L.W. Coincidence of superparamagnetism and perfect quantization in the quantum anomalous Hall state. *Phys. Rev. B* **2015**, *92*, 201304. doi: 10.1103/PhysRevB.92.201304. [[CrossRef](#)]
10. Mogi, M.; Yoshimi, R.; Tsukazaki, A.; Yasuda, K.; Kozuka, Y.; Takahashi, K.S.; Kawasaki, M.; Tokura, Y. Magnetic modulation doping in topological insulators toward higher-temperature quantum anomalous Hall effect. *Appl. Phys. Lett.* **2015**, *107*, 182401. doi: 10.1063/1.4935075. [[CrossRef](#)]
11. Wilczek, F. Two applications of axion electrodynamics. *Phys. Rev. Lett.* **1987**, *58*, 1799–1802. doi: 10.1103/PhysRevLett.58.1799. [[CrossRef](#)]
12. Qi, X.L.; Hughes, T.L.; Zhang, S.C. Topological field theory of time-reversal invariant insulators. *Phys. Rev. B* **2008**, *78*, 195424. doi: 10.1103/PhysRevB.78.195424. [[CrossRef](#)]
13. Morimoto, T.; Furusaki, A.; Nagaosa, N. Topological magnetoelectric effects in thin films of topological insulators. *Phys. Rev. B* **2015**, *92*, 085113. doi: 10.1103/PhysRevB.92.085113. [[CrossRef](#)]
14. Wang, J.; Lian, B.; Qi, X.L.; Zhang, S.C. Quantized topological magnetoelectric effect of the zero-plateau quantum anomalous Hall state. *Phys. Rev. B* **2015**, *92*, 081107. doi: 10.1103/PhysRevB.92.081107. [[CrossRef](#)]
15. Mogi, M.; Kawamura, M.; Yoshimi, R.; Tsukazaki, A.; Kozuka, Y.; Shirakawa, N.; Takahashi, K.S.; Kawasaki, M.; Tokura, Y. A magnetic heterostructure of topological insulators as a candidate for an axion insulator. *Nat. Mater.* **2017**, *16*, 516–521. doi: 10.1038/nmat4855. [[CrossRef](#)]
16. Mogi, M.; Kawamura, M.; Tsukazaki, A.; Yoshimi, R.; Takahashi, K.S.; Kawasaki, M.; Tokura, Y. Tailoring tricolor structure of magnetic topological insulator for robust axion insulator. *Sci. Adv.* **2017**, *3*, eaao1669. doi: 10.1126/sciadv.aao1669. [[CrossRef](#)]
17. Geim, A.K.; Grigorieva, I.V. Van der Waals heterostructures. *Nature* **2013**, *499*, 419–425. doi: 10.1038/nature12385. [[CrossRef](#)]
18. Novoselov, K.; Mishchenko, A.; Carvalho, A.; Castro Neto, A.H. 2D materials and van der Waals heterostructures. *Science* **2016**, *353*, aac9439. doi: 10.1126/science.aac9439. [[CrossRef](#)] [[PubMed](#)]
19. Bafekry, A.; Stampfl, C.; Faraji, M.; Yagmurcukardes, M.; Fadlallah, M.M.; Jappor, H.R.; Ghergherehchi, M.; Feghhi, S.A.H. A Dirac-semimetal two-dimensional BeN<sub>4</sub>: Thickness-dependent electronic and optical properties. *Appl. Phys. Lett.* **2021**, *118*, 203103. doi: 10.1063/5.0051878. [[CrossRef](#)]
20. Bafekry, A.; Faraji, M.; Karbasizadeh, S.; Sarsari, I.A.; Jappor, H.R.; Ghergherehchi, M.; Gogova, D. Two-dimensional FeTe<sub>2</sub> and predicted Janus FeXS (X: Te and Se) monolayers with intrinsic half-metallic character: Tunable electronic and magnetic properties via strain and electric field. *Phys. Chem. Chem. Phys.* **2021**, *23*, 24336–24343. doi: 10.1039/D1CP03078G. [[CrossRef](#)] [[PubMed](#)]
21. Liu, J.; Hesjedal, T. Magnetic Topological Insulator Heterostructures: A Review. *Adv. Mater.* **2021**, 2102427. doi: 10.1002/adma.202102427. [[CrossRef](#)]
22. Hirahara, T.; Ereemeev, S.V.; Shirasawa, T.; Okuyama, Y.; Kubo, T.; Nakanishi, R.; Akiyama, R.; Takayama, A.; Hajiri, T.; Ideta, S.I.; et al. Large-Gap Magnetic Topological Heterostructure Formed by Subsurface Incorporation of a Ferromagnetic Layer. *Nano Lett.* **2017**, *17*, 3493–3500. doi: 10.1021/acs.nanolett.7b00560. [[CrossRef](#)]
23. Otrokov, M.M.; Menshchikova, T.V.; Vergniory, M.G.; Rusinov, I.P.; Yu Vyazovskaya, A.; Koroteev, Y.M.; Bihlmayer, G.; Ernst, A.; Echenique, P.M.; Arnau, A.; et al. Highly-ordered wide bandgap materials for quantized anomalous Hall and magnetoelectric effects. *2D Mater.* **2017**, *4*, 025082. doi: 10.1088/2053-1583/aa6bec. [[CrossRef](#)]
24. Otrokov, M.M.; Menshchikova, T.V.; Rusinov, I.P.; Vergniory, M.G.; Kuznetsov, V.M.; Chulkov, E.V. Magnetic extension as an efficient method for realizing the quantum anomalous hall state in topological insulators. *JETP Lett.* **2017**, *105*, 297–302. doi: 10.1134/S0021364017050113. [[CrossRef](#)]
25. Petrov, E.K.; Silkin, I.V.; Menshchikova, T.V.; Chulkov, E.V. Cr-Containing Ferromagnetic Film–Topological Insulator Heterostructures as Promising Materials for the Quantum Anomalous Hall Effect. *JETP Lett.* **2019**, *109*. doi: 10.1134/s0021364019020127. [[CrossRef](#)]
26. Otrokov, M.M.; Klimovskikh, I.I.; Bentmann, H.; Estyunin, D.; Zeugner, A.; Aliev, Z.S.; Gaß, S.; Wolter, A.U.B.; Koroleva, A.V.; Shikin, A.M.; et al. Prediction and observation of an antiferromagnetic topological insulator. *Nature* **2019**, *576*, 416–422. doi: 10.1038/s41586-019-1840-9. [[CrossRef](#)] [[PubMed](#)]
27. Otrokov, M.M.; Rusinov, I.P.; Blanco-Rey, M.; Hoffmann, M.; Vyazovskaya, A.Y.; Ereemeev, S.V.; Ernst, A.; Echenique, P.M.; Arnau, A.; Chulkov, E.V. Unique Thickness-Dependent Properties of the van der Waals Interlayer Antiferromagnet MnBi<sub>2</sub>Te<sub>4</sub> Films. *Phys. Rev. Lett.* **2019**, *122*, 107202. doi: 10.1103/PhysRevLett.122.107202. [[CrossRef](#)]
28. Li, J.; Li, Y.; Du, S.; Wang, Z.; Gu, B.L.; Zhang, S.C.; He, K.; Duan, W.; Xu, Y. Intrinsic magnetic topological insulators in van der Waals layered MnBi<sub>2</sub>Te<sub>4</sub>-family materials. *Sci. Adv.* **2019**, *5*, eaaw5685. doi: 10.1126/sciadv.aaw5685. [[CrossRef](#)] [[PubMed](#)]
29. Zhang, D.; Shi, M.; Zhu, T.; Xing, D.; Zhang, H.; Wang, J. Topological Axion States in the Magnetic Insulator MnBi<sub>2</sub>Te<sub>4</sub> with the Quantized Magnetoelectric Effect. *Phys. Rev. Lett.* **2019**, *122*, 206401. doi: 10.1103/PhysRevLett.122.206401. [[CrossRef](#)]
30. Gong, Y.; Guo, J.; Li, J.; Zhu, K.; Liao, M.; Liu, X.; Zhang, Q.; Gu, L.; Tang, L.; Feng, X.; et al. Experimental Realization of an Intrinsic Magnetic Topological Insulator. *Chin. Phys. Lett.* **2019**, *36*, 076801. doi: 10.1088/0256-307x/36/7/076801. [[CrossRef](#)]
31. Mong, R.S.K.; Essin, A.M.; Moore, J.E. Antiferromagnetic topological insulators. *Phys. Rev. B* **2010**, *81*, 245209. doi: 10.1103/PhysRevB.81.245209. [[CrossRef](#)]

32. Liu, C.; Wang, Y.; Li, H.; Wu, Y.; Li, Y.; Li, J.; He, K.; Xu, Y.; Zhang, J.; Wang, Y. Robust axion insulator and Chern insulator phases in a two-dimensional antiferromagnetic topological insulator. *Nat. Mater.* **2020**, *19*, 522–527. doi: 10.1038/s41563-019-0573-3. [[CrossRef](#)] [[PubMed](#)]
33. Deng, Y.; Yu, Y.; Shi, M.Z.; Guo, Z.; Xu, Z.; Wang, J.; Chen, X.H.; Zhang, Y. Quantum anomalous Hall effect in intrinsic magnetic topological insulator  $\text{MnBi}_2\text{Te}_4$ . *Science* **2020**, *367*, 895–900. doi: 10.1126/science.aax8156. [[CrossRef](#)] [[PubMed](#)]
34. Gao, A.; Liu, Y.F.; Hu, C.; Qiu, J.X.; Tzschaschel, C.; Ghosh, B.; Ho, S.C.; Bérubé, D.; Chen, R.; Sun, H.; et al. Layer Hall effect in a 2D topological axion antiferromagnet. *Nature* **2021**, *595*, 521–525. doi: 10.1038/s41586-021-03679-w. [[CrossRef](#)]
35. Ge, J.; Liu, Y.; Li, J.; Li, H.; Luo, T.; Wu, Y.; Xu, Y.; Wang, J. High-Chern-Number and High-Temperature Quantum Hall Effect without Landau Levels. *Natl. Sci. Rev.* **2020**, *7*, 1280–1287. nwa089. [[CrossRef](#)] [[PubMed](#)]
36. Lei, C.; MacDonald, A.H. Gate-tunable quantum anomalous Hall effects in  $\text{MnBi}_2\text{Te}_4$  thin films. *Phys. Rev. Mater.* **2021**, *5*, L051201. doi: 10.1103/PhysRevMaterials.5.L051201. [[CrossRef](#)]
37. Petrov, E.K.; Men'shov, V.N.; Rusinov, I.P.; Hoffmann, M.; Ernst, A.; Otrokov, M.M.; Dugaev, V.K.; Menshchikova, T.V.; Chulkov, E.V. Domain wall induced spin-polarized flat bands in antiferromagnetic topological insulators. *Phys. Rev. B* **2021**, *103*, 235142. doi: 10.1103/PhysRevB.103.235142. [[CrossRef](#)]
38. Aliev, Z.S.; Amiraslanov, I.R.; Nasonova, D.I.; Shevelkov, A.V.; Abdullayev, N.A.; Jahangirli, Z.A.; Orujlu, E.N.; Otrokov, M.M.; Mamedov, N.T.; Babanly, M.B.; et al. Novel ternary layered manganese bismuth tellurides of the  $\text{MnTe-Bi}_2\text{Te}_3$  system: Synthesis and crystal structure. *J. Alloy. Compd.* **2019**, *789*, 443–450. doi: 10.1016/j.jallcom.2019.03.030. [[CrossRef](#)]
39. Hu, C.; Gordon, K.N.; Liu, P.; Liu, J.; Zhou, X.; Hao, P.; Narayan, D.; Emmanouilidou, E.; Sun, H.; Liu, Y.; et al. A van der Waals antiferromagnetic topological insulator with weak interlayer magnetic coupling. *Nat. Commun.* **2020**, *11*, 97. doi: 10.1038/s41467-019-13814-x. [[CrossRef](#)]
40. Wu, J.; Liu, F.; Sasase, M.; Ienaga, K.; Obata, Y.; Yukawa, R.; Horiba, K.; Kumigashira, H.; Okuma, S.; Inoshita, T.; et al. Natural van der Waals heterostructural single crystals with both magnetic and topological properties. *Sci. Adv.* **2019**, *5*, eaax9989. doi: 10.1126/sciadv.aax9989. [[CrossRef](#)]
41. Jahangirli, Z.A.; Alizade, E.H.; Aliev, Z.S.; Otrokov, M.M.; Ismayilova, N.A.; Mammadov, S.N.; Amiraslanov, I.R.; Mamedov, N.T.; Orudjev, G.S.; Babanly, M.B.; et al. Electronic structure and dielectric function of Mn-Bi-Te layered compounds. *J. Vac. Sci. Technol. B* **2019**, *37*, 062910. doi: 10.1116/1.5122702. [[CrossRef](#)]
42. Yan, J.Q.; Liu, Y.H.; Parker, D.S.; Wu, Y.; Aczel, A.A.; Matsuda, M.; McGuire, M.A.; Sales, B.C. A-type antiferromagnetic order in  $\text{MnBi}_4\text{Te}_7$  and  $\text{MnBi}_6\text{Te}_{10}$  single crystals. *Phys. Rev. Mater.* **2020**, *4*, 054202. doi: 10.1103/PhysRevMaterials.4.054202. [[CrossRef](#)]
43. Klimovskikh, I.I.; Otrokov, M.M.; Estyunin, D.; Ereemeev, S.V.; Filnov, S.O.; Koroleva, A.; Shevchenko, E.; Voroshnin, V.; Rybkin, A.G.; Rusinov, I.P.; et al. Tunable 3D/2D magnetism in the  $(\text{MnBi}_2\text{Te}_4)(\text{Bi}_2\text{Te}_3)_m$  topological insulators family. *NPJ Quantum Mater.* **2020**, *5*, 54. doi: 10.1038/s41535-020-00255-9. [[CrossRef](#)]
44. Vidal, R.C.; Zeugner, A.; Facio, J.I.; Ray, R.; Haghghi, M.H.; Wolter, A.U.B.; Corredor Bohorquez, L.T.; Cagliaris, F.; Moser, S.; Figgemeier, T.; et al. Topological Electronic Structure and Intrinsic Magnetization in  $\text{MnBi}_4\text{Te}_7$ : A  $\text{Bi}_2\text{Te}_3$  Derivative with a Periodic Mn Sublattice. *Phys. Rev. X* **2019**, *9*, 041065. doi: 10.1103/PhysRevX.9.041065. [[CrossRef](#)]
45. Deng, H.; Chen, Z.; Wołoś, A.; Konczykowski, M.; Sobczak, K.; Sitnicka, J.; Fedorchenko, I.V.; Borysiuk, J.; Heider, T.; Pluciński, Ł.; et al. High-temperature quantum anomalous Hall regime in a  $\text{MnBi}_2\text{Te}_4/\text{Bi}_2\text{Te}_3$  superlattice. *Nat. Phys.* **2021**, *17*, 36–42. doi: 10.1038/s41567-020-0998-2. [[CrossRef](#)]
46. Ereemeev, S.V.; Rusinov, I.P.; Koroteev, Y.M.; Vyazovskaya, A.Y.; Hoffmann, M.; Echenique, P.M.; Ernst, A.; Otrokov, M.M.; Chulkov, E.V. Topological Magnetic Materials of the  $(\text{MnSb}_2\text{Te}_4)\cdot(\text{Sb}_2\text{Te}_3)_n$  van der Waals Compounds Family. *J. Phys. Chem. Lett.* **2021**, *12*, 4268–4277. doi: 10.1021/acs.jpclett.1c00875. [[CrossRef](#)]
47. Hagmann, J.A.; Li, X.; Chowdhury, S.; Dong, S.N.; Rouvimov, S.; Pookpanratana, S.J.; Man Yu, K.; Orlova, T.A.; Bolin, T.B.; Segre, C.U.; et al. Molecular beam epitaxy growth and structure of self-assembled  $\text{Bi}_2\text{Se}_3/\text{Bi}_2\text{MnSe}_4$  multilayer heterostructures. *New J. Phys.* **2017**, *19*, 085002. doi: 10.1088/1367-2630/aa759c. [[CrossRef](#)]
48. Rienks, E.D.L.; Wimmer, S.; Sánchez-Barriga, J.; Caha, O.; Mandal, P.S.; Růžička, J.; Ney, A.; Steiner, H.; Volobuev, V.V.; Groiss, H.; et al. Large magnetic gap at the Dirac point in  $\text{Bi}_2\text{Te}_3/\text{MnBi}_2\text{Te}_4$  heterostructures. *Nature* **2019**, *576*, 423–428. doi: 10.1038/s41586-019-1826-7. [[CrossRef](#)]
49. Hirahara, T.; Otrokov, M.M.; Sasaki, T.T.; Sumida, K.; Tomohiro, Y.; Kusaka, S.; Okuyama, Y.; Ichinokura, S.; Kobayashi, M.; Takeda, Y.; et al. Fabrication of a novel magnetic topological heterostructure and temperature evolution of its massive Dirac cone. *Nat. Commun.* **2020**, *11*, 4821. doi: 10.1038/s41467-020-18645-9. [[CrossRef](#)]
50. Ereemeev, S.V.; Otrokov, M.M.; Chulkov, E.V. Competing rhombohedral and monoclinic crystal structures in  $\text{MnPn}_2\text{Ch}_4$  compounds: An ab-initio study. *J. Alloy. Compd.* **2017**, *709*, 172–178. doi: 10.1016/j.jallcom.2017.03.121. [[CrossRef](#)]
51. Blöchl, P.E. Projector Augmented-Wave Method. *Phys. Rev. B* **1994**, *50*, 17953. doi: 10.1103/PhysRevB.50.17953. [[CrossRef](#)] [[PubMed](#)]
52. Kresse, G.; Hafner, J. Ab Initio Molecular Dynamics for Liquid Metals. *Phys. Rev. B* **1993**, *47*, 558–561. [[CrossRef](#)] [[PubMed](#)]
53. Kresse, G.; Furthmüller, J. Efficient Iterative Schemes for Ab Initio Total-Energy Calculations Using a Plane-Wave Basis Set. *Phys. Rev. B* **1996**, *54*, 11169. doi: 10.1103/PhysRevB.54.11169. [[CrossRef](#)] [[PubMed](#)]
54. Kresse, G.; Furthmüller, J. Efficiency of Ab-Initio Total Energy Calculations for Metals and Semiconductors Using a Plane-Wave Basis Set. *Comput. Mater. Sci.* **1996**, *6*, 15–50. doi: 10.1016/0927-0256(96)00008-0. [[CrossRef](#)]
55. Perdew, J.P.; Burke, K.; Ernzerhof, M. Generalized Gradient Approximation Made Simple. *Phys. Rev. Lett.* **1996**, *77*, 3865. doi: 10.1103/PhysRevLett.77.3865. [[CrossRef](#)] [[PubMed](#)]



56. Koelling, D.; Harmon, B. A Technique for Relativistic Spin-Polarised Calculations. *J. Phys. Solid State Phys.* **1977**, *10*, 3107. doi: 10.1088/0022-3719/10/16/019. [[CrossRef](#)]
57. Grimme, S.; Antony, J.; Ehrlich, S.; Krieg, H. A Consistent and Accurate Ab Initio Parametrization of Density Functional Dispersion Correction (DFT-D) for the 94 Elements H-Pu. *J. Chem. Phys.* **2010**, *132*, 154104. doi: 10.1063/1.3382344. [[CrossRef](#)]
58. Marzari, N.; Vanderbilt, D. Maximally Localized Generalized Wannier Functions for Composite Energy Bands. *Phys. Rev. B* **1997**, *56*, 12847. doi: 10.1103/PhysRevB.56.12847. [[CrossRef](#)]
59. Souza, I.; Marzari, N.; Vanderbilt, D. Maximally Localized Wannier Functions for Entangled Energy Bands. *Phys. Rev. B* **2001**, *65*, 035109. doi: 10.1103/PhysRevB.65.035109. [[CrossRef](#)]
60. Mostofi, A.; Yates, J.R.; Pizzi, G.; Lee, Y.S.; Souza, I.; Vanderbilt, D.; Marzari, N. An Updated Version of wannier90: A Tool for Obtaining Maximally-Localised Wannier Functions. *Comput. Phys. Commun.* **2014**, *185*, 2309–2310. doi: 10.1016/j.cpc.2014.05.003. [[CrossRef](#)]
61. Sancho, M.P.L.; Sancho, J.M.L.; Sancho, J.M.L.; Rubio, J. Highly Convergent Schemes for the Calculation of Bulk and Surface Green Functions. *J. Phys. F Met. Phys.* **1985**, *15*, 851–858. doi: 10.1088/0305-4608/15/4/009. [[CrossRef](#)]
62. Wu, Q.; Zhang, S.; Song, H.F.; Troyer, M.; Soluyanov, A. WannierTools : An Open-Source Software Package for Novel Topological Materials. *Comput. Phys. Commun.* **2018**, *224*, 405–416. doi: 10.1016/j.cpc.2017.09.033. [[CrossRef](#)]
63. Anisimov, V.I.; Zaanen, J.; Andersen, O.K. Band Theory and Mott Insulators: Hubbard  $U$  Instead of Stoner  $I$ . *Phys. Rev. B* **1991**, *44*, 943–954. doi: 10.1103/PhysRevB.44.943. [[CrossRef](#)]
64. Dudarev, S.; Botton, G.; Savrasov, S.; Humphreys, C.; Sutton, A. Electron-Energy-Loss Spectra and the Structural Stability of Nickel Oxide: An LSDA+ $U$  Study. *Phys. Rev. B* **1998**, *57*, 1505–1509. doi: 10.1103/PhysRevB.57.1505. [[CrossRef](#)]
65. Youn, S. Calculation of the Hubbard  $U$  parameters by the solid atom method. *J. Magn.* **2005**, *10*, 71–75. [[CrossRef](#)]
66. Cococcioni, M.; de Gironcoli, S. Linear response approach to the calculation of the effective interaction parameters in the LDA +  $U$  method. *Phys. Rev. B* **2005**, *71*, 035105. doi: 10.1103/PhysRevB.71.035105. [[CrossRef](#)]
67. Soluyanov, A.A.; Vanderbilt, D. Computing topological invariants without inversion symmetry. *Phys. Rev. B* **2011**, *83*, 235401. doi: 10.1103/PhysRevB.83.235401. [[CrossRef](#)]
68. Gresch, D.; Autès, G.; Yazyev, O.V.; Troyer, M.; Vanderbilt, D.; Bernevig, B.A.; Soluyanov, A.A. Z2Pack: Numerical implementation of hybrid Wannier centers for identifying topological materials. *Phys. Rev. B* **2017**, *95*, 075146. doi: 10.1103/PhysRevB.95.075146. [[CrossRef](#)]
69. Ereameev, S.V.; Koroteev, Y.M.; Chulkov, E.V. Effect of the atomic composition of the surface on the electron surface states in topological insulators  $A_2^V B_3^VI$ . *JETP Lett.* **2010**, *91*, 387–391. doi: 10.1134/S0021364010080059. [[CrossRef](#)]